Manuscript refereed by Mr Alexander Angré (Carpenter Powder Products AB, Sweden)

Tailor-Made Functional Composite Components Using AM and HIP

Riehm, Sebastian[1] (s.riehm@iwm.rwth-aachen.de); Friederici, Vera[2] (vera.friederici@ifam.fraunhofer.de); Herzog, Simone[1] (s.herzog@iwm.rwth-aachen.de); Kaletsch, Anke[1] (a.kaletsch@iwm.rwth-aachen.de); Broeckmann, Christoph[1] (c.broeckmann@iwm.rwth-aachen.de)

[1]RWTH Aachen University, IWM, Augustinerbach 4, 52062 Aachen, Germany
[2]Fraunhofer IFAM, Wiener Straße 12, 28359 Bremen, Germany

Abstract
The combination of Additive Manufacturing (AM) and Hot Isostatic Pressing (HIP) offers great potential for industrial applications. Skillfully connecting AM and HIP creates a manufacturing process that unites the advantages of both processes. We demonstrate a production route for composite components by AM + HIP. A capsule made of wear-resistant or corrosion-resistant steel is additively manufactured by Laser-Powder Bed Fusion (LPBF). Before building, the geometry of the capsule is optimized by FEM simulation to obtain a desired shape. In a second step, the capsule is filled with structural steel powder and sealed in a conventional powder HIP process. The capsule remains on the component as an outer layer. In this way a complex-shaped, functional net shape composite component is produced. The composite components created by this route are characterized by metallographic investigations.

1. Introduction

Laser Powder Bed Fusion (LPBF) and Hot Isostatic Pressing (HIP) are two flexible powder-metallurgical (PM) process routes to produce high-quality metallic components. While HIP has established its place over the last decades, LPBF as one possibility of Additive Manufacturing (AM) is just gaining popularity. [1, 2]

HIP is the only process route that is capable of producing fully dense powder-metallurgical components [3]. That is why HIP is of utmost importance for highly stressed components. When the optimal parameter combination of temperature, pressure and holding time for a specific material is used, inner pores and voids can be virtually eliminated by HIP. Occasionally there may still be pores in the size range of several nanometres after HIP [4]. Densifying components in such a way that they are free of pores has a very positive effect on their mechanical properties like fatigue strength, hardness or toughness [5–7].

Two HIP process routes are possible: With powder HIP, powder is filled into a deformable can and consolidated to full density. The can will shrink approximately up to 30% in size because of the densification. The HIP'ed capsule can be further processed as semi-finished product or has already reached net-shape geometry. The second field of application of HIP is post-densification of solid components that exhibit voids of residual porosity. For example after casting or pressing, components can be HIP'ed to full density. [8]

One big advantage of LPBF is its capability of building very complex net-shape components, while conventional cans for powder HIP are restricted to comparatively simple geometries. On the other hand, the size of current LPBF machines very much limits the size of components to be built. Moreover, although LPBF can be easily integrated into the CAD/CAM process chain, the building of each component takes a very long time. [9]

In order to combine the respective advantages of both LPBF and HIP while at the same time overcoming some of the deficiencies, both process routes can be combined. One approach is presented in this study: Open, thin-walled HIP capsules are built by LPBF. In a following step, they are filled with powder and exhibited to a conventional powder HIP process. With this combination complex-shaped capsules can be built and HIP'ed in comparatively short time, because only thin walls have to be built by LPBF. Another advantage stems from the choice of materials: Capsule and bulk can be made from two different but complemental materials. In this way it is possible to manufacture composite components with a complex, net-shape geometry and tailored properties.

© European Powder Metallurgy Association (EPMA)

2. Materials and Experiments

In this study, composite components with either a corrosion resistant or wear resistant outer surface as well as a tough core are to be produced by combining LPBF and HIP. The materials were selected not only for their suitability for the processes but also for their industrial and scientific relevance.

Materials and Powder Properties

In Table 1 the selected materials and their combinations are shown, that are investigated in the context of this study.

Table 1: Material selection.

	Capsule	Bulk
Monolithic 1	Austenitic stainless steel AISI 316L (DIN X2CrNiMo17-13-2)	
Monolithic 2	Martensitic tool steel AISI L6 (DIN 56NiCrMoV7)	
Composite 1	Austenitic stainless steel AISI 316L (DIN X2CrNiMo17-13-2)	Martensitic heat-treatable steel AISI L6 (DIN 56NiCrMoV7)
Composite 2	Carbide rich, wear resistant steel AISI A11 (DIN X245VCrMo8-5-1)	Martensitic heat-treatable steel AISI L6 (DIN 56NiCrMoV7)

The first experiments were conducted with monolithic capsules where capsule material is the same as bulk material. The focus of this study, however, is on two material composites: The capsule is either made from corrosion resistant austenitic stainless steel AISI 316L (DIN X2CrNiMo17-13-2) or from wear resistant carbide rich tool steel AISI A11 (DIN X245VCrMo8-5-1). 316L is used for example in machined parts such as pipe fittings or valves in chemical, pharmaceutical and biological applications, where corrosion resistance is needed. Because of its wear resistance, A11 is used for punches and dies, for knives, blades and cutters, for powder compaction tools and more. Table 2 gives the chemical composition of the investigated materials measured at IFAM Bremen. Ferritic steel powder 430L (DIN X6Cr17) is added to A11 powder in order to build crack-free samples via LPBF, see chapter 3.1.

Table 2: Chemical composition of investigated materials in wt.-% (each balance: Fe).

	C	Si	Mn	P	S	Cr	Ni	Mo	Cu	V	N	B	O
L6	0.52	0.28	0.96	<0.01	0.002	1.22	1.99	0.5	–	0.11	–	–	–
316L LPBF	0.03	0.66	0.31	0.051	0.007	16.5	13.1	2.24	–	–	0.022	–	0.051
316L HIP	0.021	0.8	0.95	0.009	0.004	17.3	13.2	2.5	0.05	–	0.14	0.001	–
A11	2.45	0.98	0.42	0.02	0.087	5	–	1.49	–	8.28	0.098	–	0.035
430L	<0.018	–	–	–	–	16–18	–	–	–	–	–	–	–

All used steel powders were analysed using standard test methods at either IWM or IFAM. The nominal fraction specified by the supplier, powder size distribution (according to ISO 13320), tap density (according to DIN EN ISO 3953) and apparent density (according to DIN EN ISO 3923-1) are given in Table 3. The powder was supplied by H.C. Starck (L6), Deutsche Edelstahl-Werke (316L LPBF; A11), Carpenter Powder Products (316L HIP) and Sandvik Osprey (430L).
For L6 and 316L, two respective fractions are listed. The finer fraction is used for building the capsules with LPBF, while the coarser fraction is intended for capsule filling. In the case of L6 one batch of gas atomised powder was sieved into three fractions (the finest fraction below 20 µm was not used). For 316L, two different powder batches from different suppliers were used.

© European Powder Metallurgy Association (EPMA)

Table 3: Powder size distribution, tap density ρ_t and apparent density ρ_a.

Material	Nominal fraction	D10	D50	D90	ρ_t	ρ_a
	µm	µm	µm	µm	g cm^{-3}	g cm^{-3}
L6 LPBF	-63 +20	33	49	68	5.0	4.2
L6 HIP	-300 +63	95	190	369	5.0	4.5
316L LPBF	-53 +20	26	40	56	5.1	4.6
316L HIP	-500 +0	88	199	394	5.6	5.0
A11	-53 +20	32	42	55	4.9	4.2
430L	-45 +10	18	38	53	—	—

2.1. LPBF and HIP

The parameter studies and capsule building were done at IFAM Bremen using an LPBF unit “M270 Dual Mode” from EOS GmbH (Munich/Germany). This unit is equipped with a powder bed heating of up to 300 °C. LPBF building is performed in pure nitrogen atmosphere with max 0.3% oxygen content. HIP cycles were conducted at IWM Aachen with a HIP unit “Shirp 20/30-200-1500” by ABRA Fluid AG (Widnau/Switzerland). Process gas for HIP is Argon.
The process chain of building composite components with LPBF and HIP is depicted in Figure 1: Starting from metal powder (1), a laser beam builds up the capsule layer-by-layer into the powder bed (2). After completing the built-up the capsule is withdrawn from the LPBF unit. Residual powder and supporting structure are removed (3). The capsules are built with a small socket at the open end. In the next step, a filling and evacuation tube is welded to this socket (4). The capsule is filled with powder, evacuated and sealed through the filling tube (5, 6). After HIP (7), the composite component is completed (8).

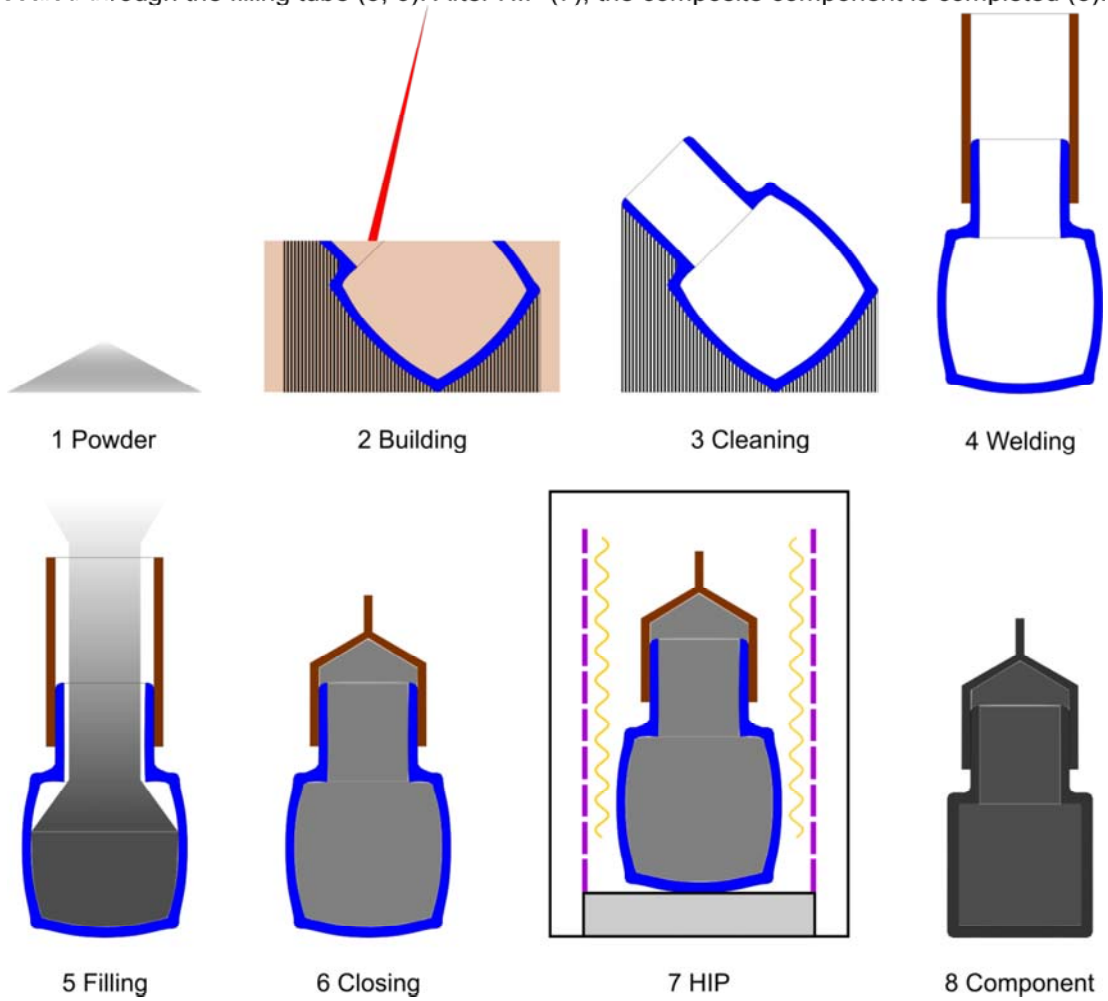


Figure 1: Process chain of building components with LPBF and powder HIP.

© European Powder Metallurgy Association (EPMA)

2.1.1. Capsule Building

The LPBF process is influenced by a number of parameters like layer thickness, temperature of the building plate, laser parameters or scanning strategy. In order to find the optimal LPBF parameters for building capsules out of the intended materials, the best combination has to be determined.
At the beginning of parameter optimization, parameter values were chosen based on former studies and literature. Different parameters for laser power were combined with different parameters of scanning speed. The first built components were solid cubes (edge length: 5 mm) and single walls (thickness 0.5 mm, length 10 mm, height 5 mm). These simple components were then examined metallographically with regard to pores, bonding defects and cracks. The parameter set which produced as few cracks and pores as possible was selected for further optimization.
The next step involved the production of so-called benchmarking components. These benchmarking components are for example arches, overhangs, angles and hollow cubes. Additionally, contour und skin parameters were introduced in order to optimize the structure of the components and the building.
After fine-tuning the parameters HIP capsules could be finally built. The last step consisted of optimizing the positioning of the capsules on the building plate as well as optimizing the support structure.
Crucial for successful HIP of capsules is absolute gas tightness: The capsules must not have one single leak. Otherwise the pressure applied during HIP would not be able to compress and densify the component. In conventional cans for powder HIP, mostly the welds are the weak points that are examined for gas tightness. With the LPBF-built capsules, each individual wall has to be completely leak-proof. For this reason, several capsules with wall thicknesses reaching from 0.2 mm to 1.5 mm were built. These capsules had a simple cylindrical shape (diameter 15 mm, height 30 mm), were made out of 316L and had already been closed during built-up. One after another, they were put into a gas pycnometer “AccuPyc 1330” (Micromeritics Instrument Corp., Norcross/USA). If the walls were leak-proof, the device would calculate the real density of each capsule. As the capsules were filled with loose powder, the determined density would not be the full density of 316L (> 7.9 g cm^{-3}), but very close. When the wall thickness was too thin and hence the capsule was leaking, the gas pycnometer would detect too small a volume for the capsule. This would result in the displayed density being below the real density. [10] This study is a fast possibility to determine the minimal wall thickness for LPBF-built capsules needed for gas-tightness.

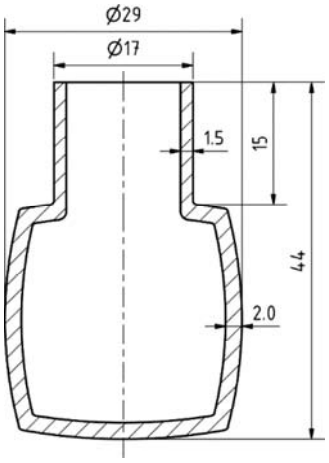


Figure 2: Geometry of a test capsule.

The geometry of the final test capsules used for LPBF and HIP experiments is shown in Figure 2. The upper wall thickness of 1.5 mm is kept constant for all capsules. This wall thickness is necessary in order to attach the filling pipe by means of TIG welding. The wall thickness of the capsule body (here denoted with 2.0 mm) is varied between 1.0 mm, 1.5 mm and 2.0 mm.

2.1.2. Hot Isostatic Pressing

The parameters that can be influenced for a HIP cycle essentially are temperature, pressure and holding time. HIP temperature should be more than 70% of solidus temperature. For high-temperature alloys, HIP temperature can even be close to the solidus temperature. The HIP pressure has to be higher than the respective yield stress at HIP temperature. Typical HIP pressures are in the range of 100 to 200 MPa. [1, 11]
After LPBF building, the capsules were cleaned with isopropyl alcohol. A filling pipe of 304L was TIG welded to the upper socket. The volume of each capsule was determined by filling the capsule with water and measuring the weight difference. A minimum mass of powder has been calculated according to the tap density of the powder and the volume of the capsule. The capsules were filled with the respective minimum powder mass or even more. After filling, the powder density inside the capsules was calculated. Relative filling densities between 61% and 65% were reached. Finally, the capsules were evacuated and sealed. HIP parameters were set based on literature and experiences to T_{HIP} = 1150 °C, p_{HIP} = 110 MPa and t_{Hold} = 3 h [12–14]. Pressure was applied when the temperature reached 750 °C. This type of cycle prevents the pressure on the capsule from being too high at low temperatures, resulting in cracks in the capsule [11].

2.2. Microstructural investigations

After HIP the grain sizes of capsule wall and filling are investigated. This is done by image analysis (IA) with the software package Fiji [15]. The capsules were prepared for IA by cutting, polishing and etching to highlight the grain boundaries. 316L is etched with Beraha III (15 s) or V_2A pickle (65 °C, 2 min); L6 is etched with a mixture of 45 ml H_2O, 45 ml HCl (37%), 6 ml HNO_3 (65%) and 8 ml HF for 5 minutes.

© European Powder Metallurgy Association (EPMA)

After etching, several images of wall and bulk are taken. The grain boundaries are redrawn by hand. After the scale is given, Fiji calculates the area of each grain from the traced grain boundaries. Every detected area with a size of less than 10 px^2 is dismissed from the results. Based on standard DIN EN ISO 643 [16], the equivalent index of grain size *G* can be calculated.

2.3. Numerical Simulation of HIP Shrinkage and HIP Densification

Shrinkage and densification during HIP can be numerically calculated using Finite Element Method (FEM) with a simulation routine developed at IWM [13]. The simulation model uses a macroscopic continuum simulation approach. The total strain is calculated according to equation (1) as:

$$\epsilon_{ij} = \epsilon_{ij}^{elastic} + \epsilon_{ij}^{plastic} + \epsilon_{ij}^{creep1} + \epsilon_{ij}^{creep2} + \epsilon_{ij}^{thermal} \quad (1)$$

For calculating the plastic deformation (time independent inelasticity) $\epsilon_{ij}^{plastic}$, Kuhn and Downey's model is used [17]. The viscoplastic deformation (rate dependent inelasticity) $\epsilon_{ij}^{creep1} + \epsilon_{ij}^{creep2}$ during primary and secondary creep respectively is calculated according to the works of Abouaf and Chenot [18].
The simulation model is implemented as user subroutine for the FEM software Abaqus. Input parameters are temperature and pressure profiles, a set of material specific parameters, relative powder density inside the capsule and the geometry of the capsule.

3. Results and Discussion

3.1. LPBF of Capsules

316L is regularly used for LPBF experiments and studies [19–21]. Based on literature and own studies laser power *P* was varied from 127.5 W to 195 W and scanning speed *v* was varied from 510 mm s^{-1} to 897 mm s^{-1} for the optimization studies. The layer thickness was set to 40 µm and hatch distance to 0.1 mm. All parameter combinations resulted in stable and crack-free walls and solid cubes. In contrast, huge differences in residual porosity and lack of fusion was investigated between the individual parameter sets. Finally, the best parameter set was determined to be *P* = 172.5 W and v_s = 690 mm s^{-1}, contour and post contour *P* = 165 W, *v* = 483 mm s^{-1}. Figure 3 shows some benchmarking components from the parameter studies (left) and a cross section of a solid cube built with the aforementioned parameters. Some small and large pores can still easily be seen.

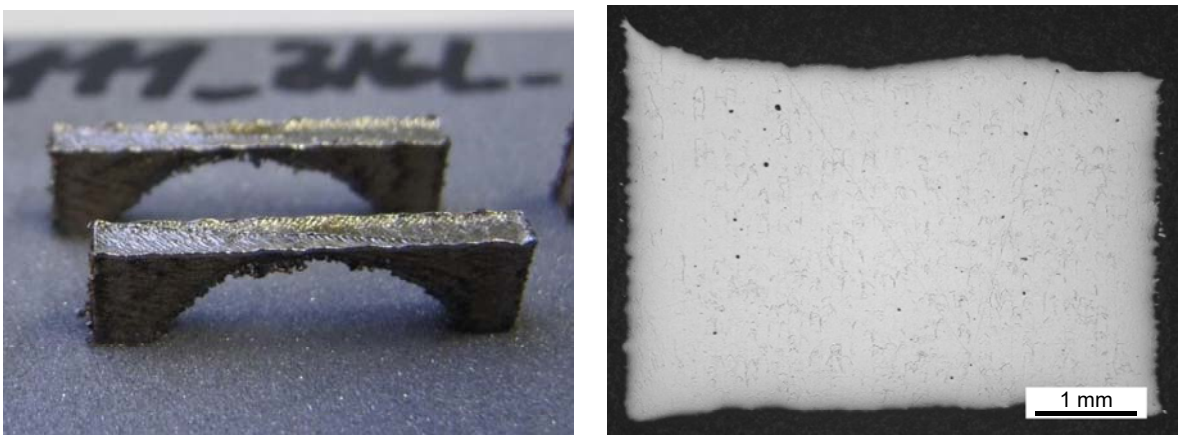


Figure 3: 316L benchmarking geometry (left) and cube (*P* = 172.5 W and *v* = 690 mm s^{-1}) (right).

For L6 the procedure was basically the same: at first walls and solid cubes, then benchmarking components, and finally optimized parameters. For the optimization studies, laser energy was kept constant at *P* = 195 W, while scanning speed was varied from *v* = 50 mm s^{-1} to *v* = 600 mm s^{-1}.After final optimization the parameters were set to *v* = 650 mm s^{-1}, *P* = 195 W, contour *v* = 360 mm s^{-1}, and post contour *v* = 240 mm s^{-1}. In Figure 4 a building plate with successfully built benchmarking components out of L6 (left) as well as a solid cube built with the optimal parameter set (right) are shown.

© European Powder Metallurgy Association (EPMA)

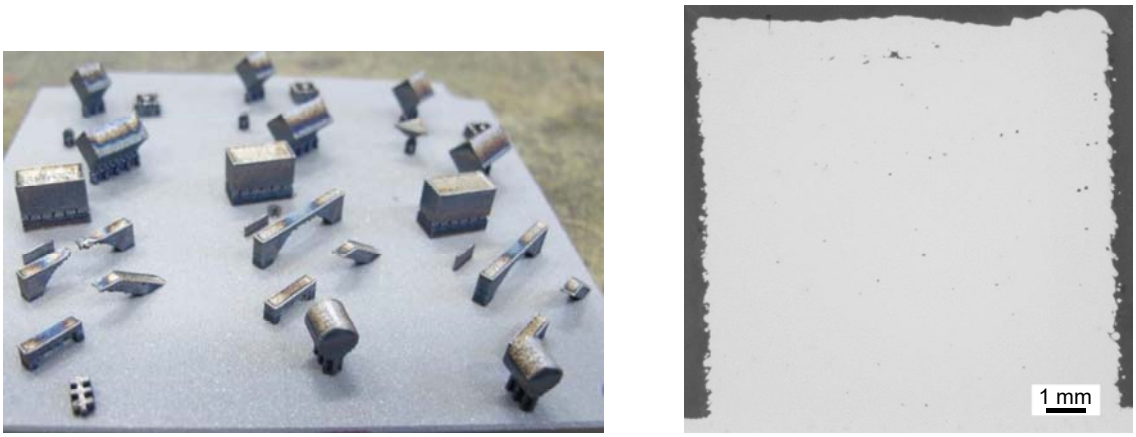


Figure 4: L6 benchmarking geometry (left) and cube (P = 195 W and v = 690 mm s^{-1}) (right).

The results of the gas pycnometry measurements are shown in Figure 5. The calculated density of each sample cylinder made from 316L according to its wall thickness is depicted. It can be seen that for 1.0 mm and above, the measurements yield the theoretical density of just below 7.9 g cm^{-3}. For capsules with a wall thickness below 1.0 mm the calculated density is much too low, exactly according to theory (see chapter 2.1.1). These measurements indicate that the minimum wall thickness to achieve gas tightness is 1 mm. The measurements were carried out with 316L, but for other materials the same should apply.

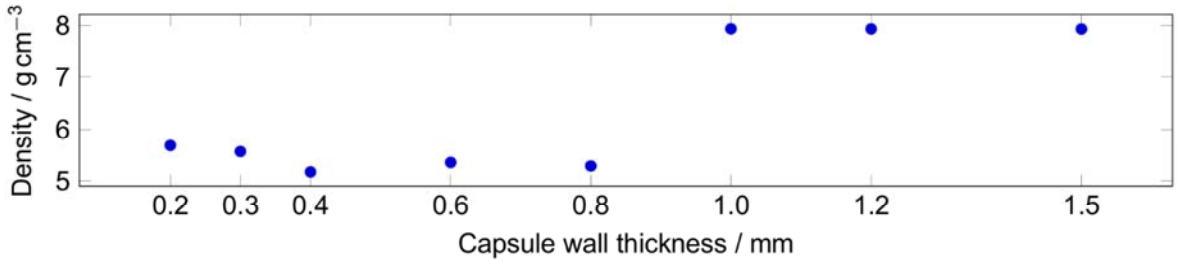


Figure 5: Results of gas pycnometry depending on wall thickness for 316L.

Using the optimized parameter sets for 316L and L6 enables to build gas tight and crack free capsules with LPBF. Figure 6 shows some of these capsules. However, the building job had to be cancelled at some point. The reason for this is the capsule geometry which exhibits a sharp-edged transition between capsule body and small socket. Due to residual stresses the sharp edges bent upwards. This lead to the fact that the roller was not able anymore to evenly distribute new powder. Redesigning the transition with a chamfer might help to avoid these problems.

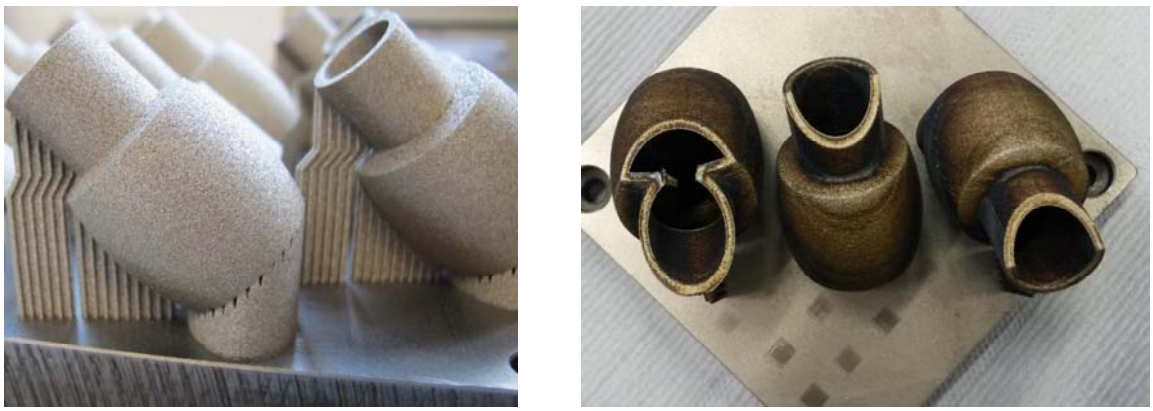


Figure 6: LPBF-built capsules of 316L (left) and L6 (right) still attached to building plate.

Processing of A11 with LPBF, on the other hand, caused problems right from the beginning. Except for very small structures like lines, LPBF building of pure A11 was not successful. Cracks as well as delaminations occur and edges or plates bend upwards.

© European Powder Metallurgy Association (EPMA)

During LPBF cooling rates of up to 10^8 K s^{-1} occur. [22] These rapid cooling rates lead to high temperature gradients between the first upper layers and the layers beneath. The stresses induced by these temperature gradients are high enough to cause cracks in brittle materials like A11. A11 is particularly brittle due to its high carbon content and the carbide-forming elements vanadium and chromium. V and Cr carbides reduce the toughness of the steel.
Thermo-Calc simulations show that around 0.8 wt.-% C is dissolved in austenite, while the remaining C is bound in carbides, see Figure 8. Because of this high C content, A11 tends to form martensite when cooling down. As the formation of martensite induces high stresses, cracks and delaminations occur after LPBF. Using several parameter combinations not even simple geometries out of A11 could be built. With a higher substrate temperature of 150 °C, cubes could be built up to approximately 1 mm in height. Above this height, cracks and delaminations destroyed the components.
Two possible solutions were examined: First, an additional heating unit enabled a substrate temperature of up to 300 °C. This will lead to smaller temperature gradients, thus to less stresses and no cracks at best-case scenario. According to the time-temperature-transformation diagram of A11 [23], this heating should be also sufficient to build above martensite start temperature.
Actually, solid cubes with an edge length of 5 mm could be built. But after cooling, all of them exhibited deep cracks, some of which reached almost through the entire component.
The second possible solution is alloy customization. In order to decrease the overall carbon content and thus enable crack-free LPBF-building, high-carbon A11 powder was pre-mixed with low-carbon ferritic steel 430L powder. This route was also partially successful. If the mixing ratio was at least 17.5 wt.-% 430L : 82.5 wt.-% A11 and the substrate temperature was 300 °C, cubes of edge length 5 mm could be built, demonstrated in Figure 7. Only few cracks or delaminations still occurred. However, not all commercial LPBF units are equipped with a heating system for such high temperatures. With 80 °C substrate temperature, cubes could be also built. In this case, the mixing ratio had to be increased to 50:50.

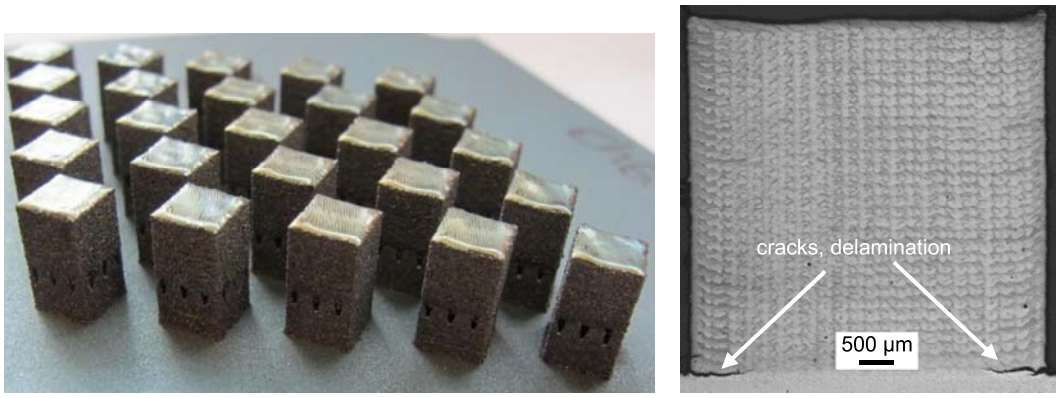


Figure 7: Cubes made of A11 with 30 wt.-% 430L (left) and 17.5 wt.-% 430L (right).

Capsules made of A11 are expected to be used as wear resistant components. As such, an appropriate C content is crucible for the formation of carbides as well as for heat-treating the matrix. Thermo-Calc simulations (see Figure 8 left) show that for pure A11, around 0.8 wt.-% C is dissolved in austenite. This slowly declines to around 0.6 wt.-% when the mixing ratio is 50:50. At the same time the amount of VC drops to less than a third. When at least 28 wt.-% of 430L is used, carbides of the type M_7C_3 start to form which are assumed to be Cr carbides. At 50:50, the sum of VC and M_7C_3 is roughly half the amount of VC at the beginning. Since the Thermo-Calc calculations assume a state of equilibrium but the LPBF process is highly turbulent, the simulations can only provide an approximation and need to be verified experimentally.
Figure 8, right, shows how the hardness HV10 changes with increasing content of 430L. Up to about 25 wt.-% of 430L the hardness hardly changes. After that, it drops and at 50:50 only about half of the starting value can be measured.

© European Powder Metallurgy Association (EPMA)

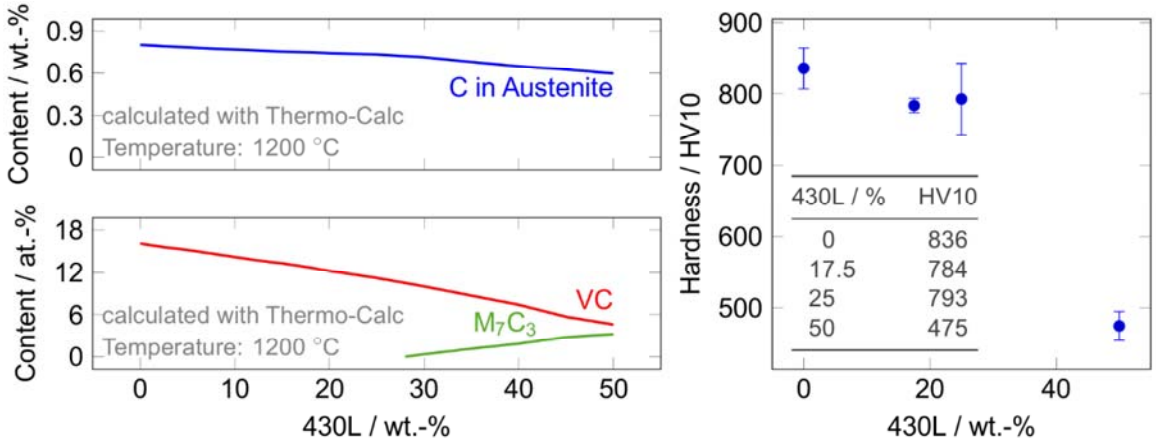


Figure 8: Influence of mixing 430L and A11 on C and carbide content (left) and hardness (right).

3.2. HIP of Capsules

Capsules before and after HIP are shown in Figure 9. On the left side, LPBF-built capsules attached with a filling tube and sealed can be seen. The same capsules deformed after HIP are depicted on the right. The diagram in the center shows the actual temperature and pressure progression from the HIP cycle.

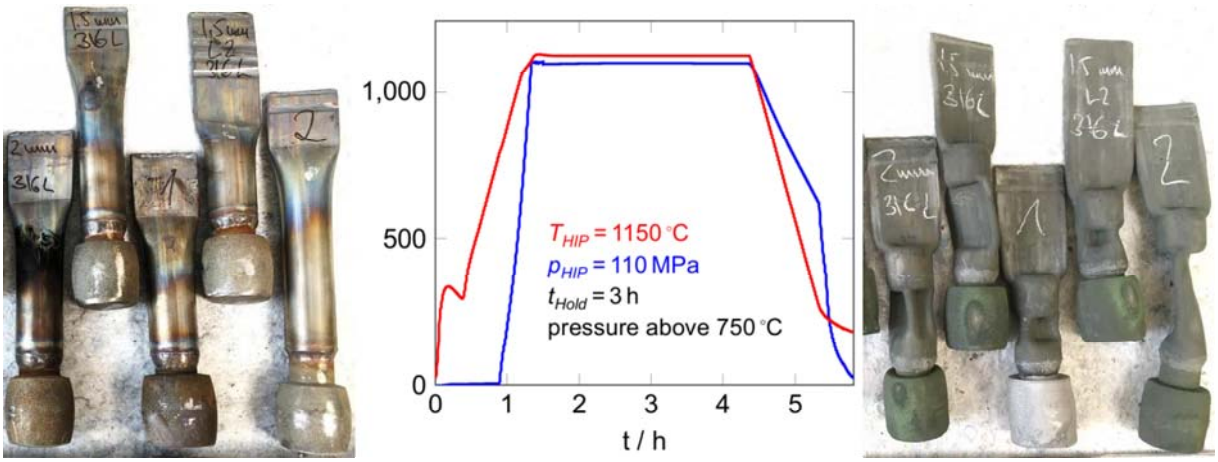


Figure 9: Capsules before (left) and after (right) HIP; log of HIP cycle (center).

3.3. Microscopic Investigations

Metallographic etched (cf. chapter 2.2) cross-cuts of two capsules after HIP are shown in Figure 10 and Figure 11 respectively. In Figure 10, capsule and bulk material is 316L. For the capsule depicted in Figure 11, 316L was used as capsule material and L6 for filling. Both capsules' nominal wall thickness is 1 mm. The LPBF building direction is shown in each figure.

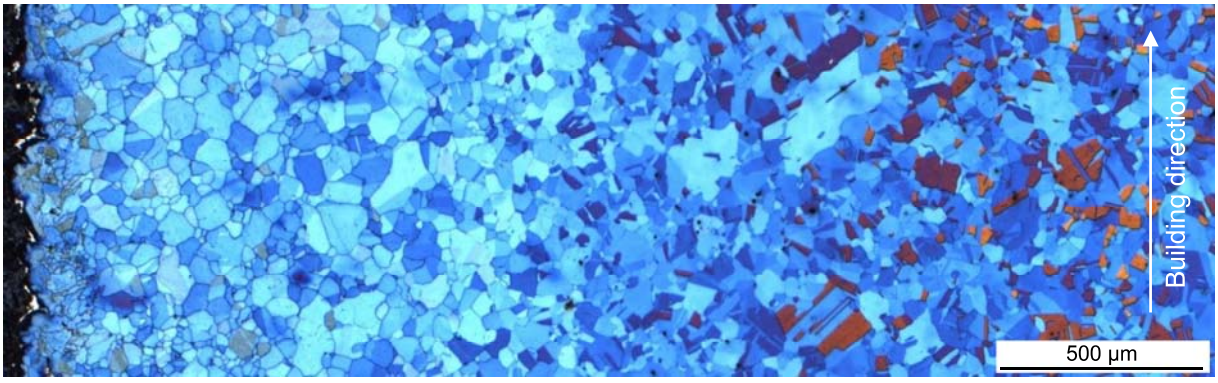


Figure 10: Microstructure after HIP: wall 316L, bulk 316L, 1 mm wall thickness.

© European Powder Metallurgy Association (EPMA)

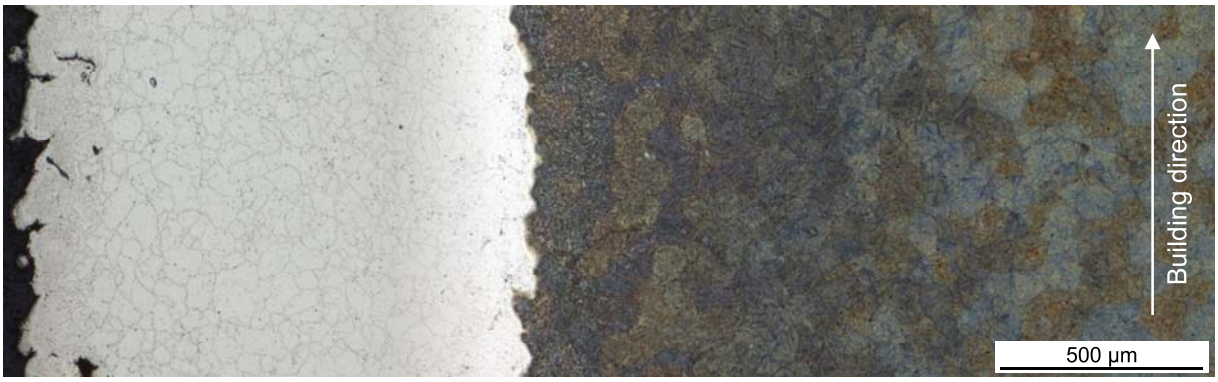


Figure 11: Microstructure after HIP: wall 316L, bulk L6, 1 mm wall thickness.

For wall 316L / bulk 316L, a distinct transition after HIP is not visible anymore. The structure seems to have joined together across both areas. For 316L / L6, there is still a harsh transition zone visible. From the figures it is also obvious that the walls after LPBF are thicker than nominally expected. In Figure 11 it can be measured that the wall is around 20% thicker. Furthermore at the outside there are voids and pores reaching more than 100 µm to the inside. These irregularities have to be considered when designing real industrial components.
For capsules made of 316L / 316L with a wall thickness of 1.0 mm, 1.5 mm or 2.0 mm respectively, the progression of Vickers hardness HV0.05 from the outside to the inside is depicted in Figure 12. Due to the rough outer surface, it was difficult to align the images accurately. The starting point of each curve may therefore be shifted by a few microns.
It can be seen that the hardness curves start with a high value near the capsule's outside. After this initial value, the hardness decreases in the area of the LPBF-built wall. Further inside behind the nominal wall thickness, the hardness increases again and remains at this value.

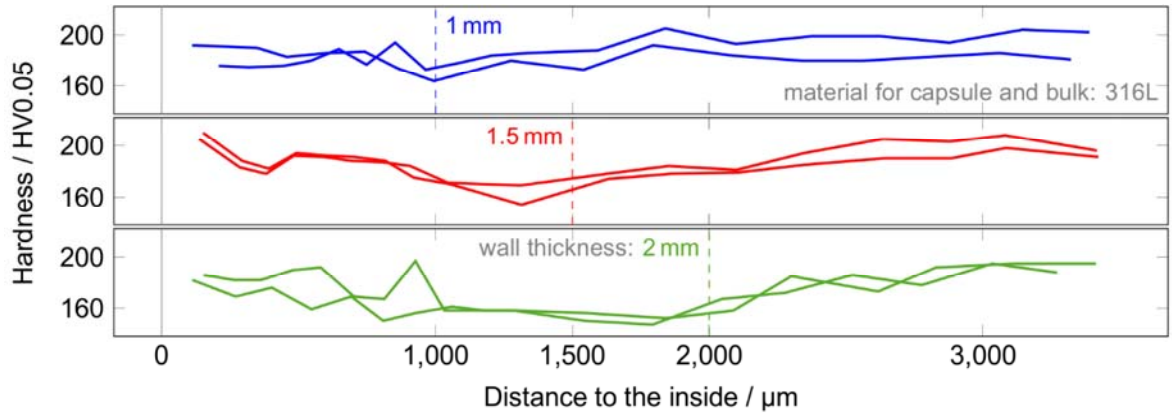


Figure 12: Hardness progression from outside to inside of different 316L / 316L capsules after HIP.

The grain sizes after HIP determined by image analysis using Fiji software are given in Table 4. The mean grain size $\bar{a}$ of wall and bulk of a 316L / 316L capsule are almost the same size after HIP, even though the initial powder fractions of LPBF and HIP were very different. It appears that recrystallization has made the grains grow to an equal size. The relatively large standard deviation is due to the fact that there are both many very small and many very large grains.
For 316L / L6, the grain sizes are largely different. The L6 bulk grains are several times as big as the grains of the 316L capsule. A very large standard deviation can also be observed here.

© European Powder Metallurgy Association (EPMA)

Table 4: Apparent grain size after HIP ($\bar{a}$: mean area of grain, SD: standard deviation; n: number of measured grains; G: equivalent index of grain size).

Material		$\bar{a}$	SD	n	G
		µm²	µm²	–	–
No. 1	316L Wall	839	1055	2266	7.2
	316L Bulk	724	1194	2628	7.4
No. 2	316L Wall	1595	1826	705	6.3
	L6 Bulk	6468	5498	799	4.3

The statistical distribution of the grain sizes is shown in greater detail in Figure 13. Each boxplot represents one of the four investigated areas. The boxes show values for median (0.5-quantile of the grain sizes), lower (0.25-quantile) and upper (0.75-quantile) quartile. The upper/lower whisker at the outer edges are calculated according to: upper/lower quartile ± 1.5 · (upper quartile − lower quartile). The mean grain size $\bar{a}$ is indicated by ♦, and outliers beyond whiskers are indicated by |.
The boxplots show that there are a lot of grains smaller than the average values. On the other hand, there are also a number of very large grains whose size is even beyond the upper whiskers.
It is remarkable that the mean grain size of the two 316L walls is not the same. The wall thickness had the same value of 1 mm, so there should be no size dependency. Two possible explanations are that the number of counted grains (2266 to 705) and thus the statistics are too different or that the etching has made the grain boundaries visible only to varying degrees. Further investigations are planned to determine the grain sizes more precisely with EBSD.

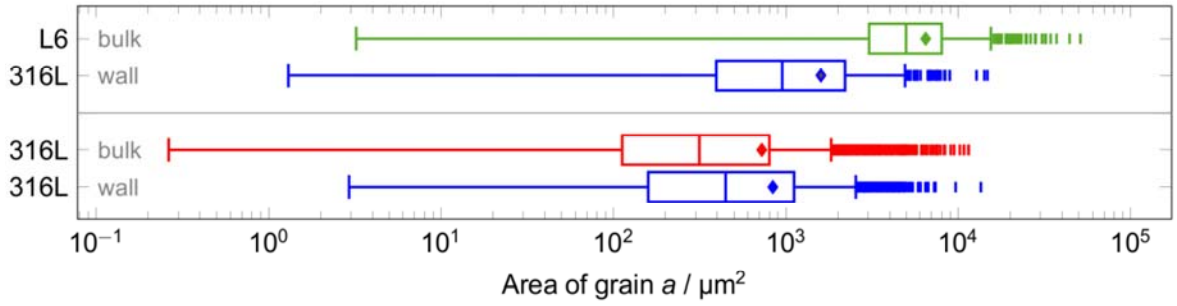


Figure 13: Statistical distribution of grain sizes.

A closer look at the transition zone of a 316L / L6 capsule is shown in Figure 14. Every number shows the approximate position of a single EDX (energy dispersive X-ray spectroscopy) measurement. Locations 1, 8 and 9 are out of scope of the figure. The results of the EDX measurements are shown in Figure 15. Obviously, Ni and Cr diffused between 316L and L6. The width of this diffusion zone is approximately 20 µm to 30 µm. Further mechanical tests have to show whether the diffusion zone has an influence on the bonding of the two materials.
On the right-hand side of Figure 14, a detail of 316L is shown. The right edge of the figure is located about 120 µm from the transition to L6. Defects of up to 10 µm in size are visible. At present, the origin of the defects cannot be identified with absolute certainty. They could be due to metallographic preparation, contaminations of the starting material or the LPBF or HIP process, or inadequate process parameters.

© European Powder Metallurgy Association (EPMA)

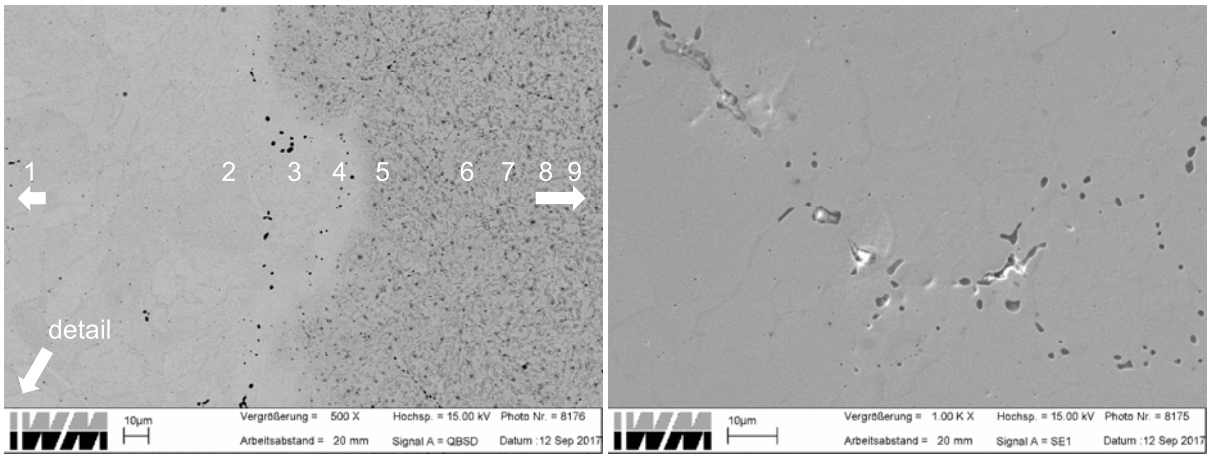


Figure 14: Transition zone of a 316L / L6 capsule (left); defects near the transition (right).

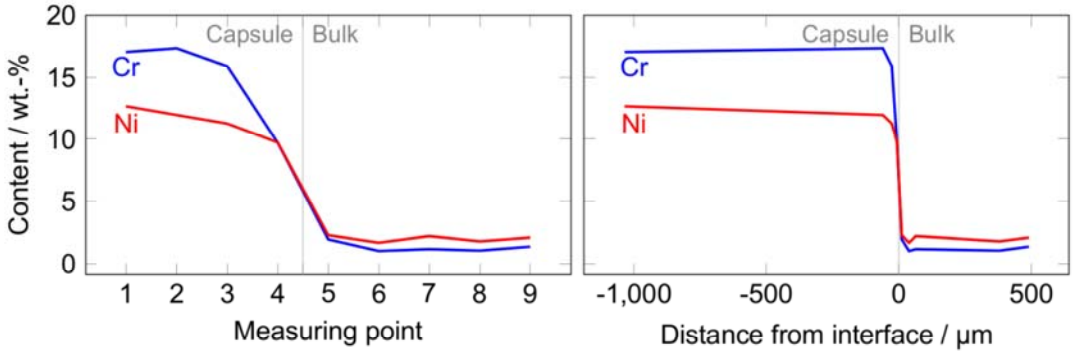


Figure 15: Distribution of Cr and Ni along transition of 316L / L6 in dependence of measuring points according to Figure 14 (left) and converted to actual distances (right).

3.4. Numerical Simulation

Densification and shrinkage and thus shape change of a capsule through HIP can be simulated by FEM. In Figure 16, a cross-cut of a 316L / 316L capsule with a wall thickness of 1 mm after HIP is shown. The original shape of this capsule can be seen in Figure 2. In the center of Figure 16, the contour of this capsule (red) is compared to the contour of a simulated capsule (black).

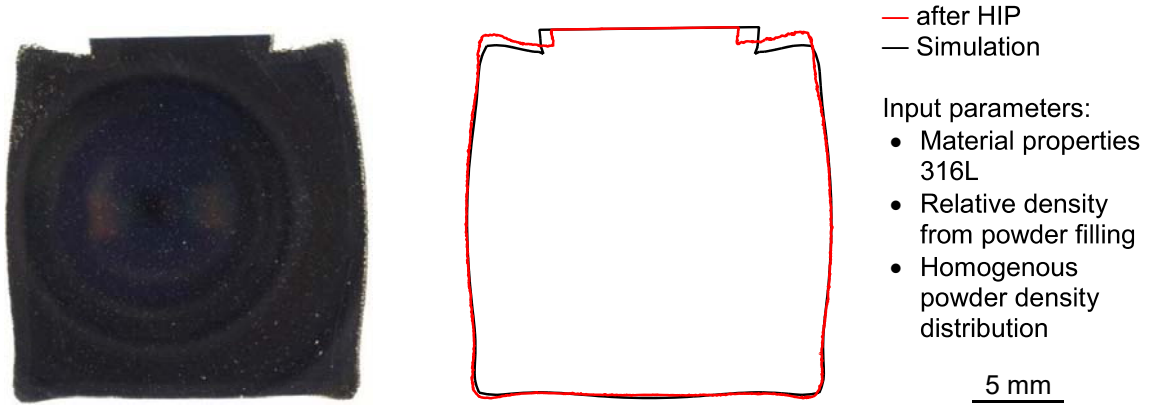


Figure 16: Comparison of 316L / 316L capsule after HIP (left) and simulation (center).

The simulation is well capable of qualitatively and quantitatively calculating the shape change of a HIP capsule. The welded filling tube at the upper socket leads to more stiffness and irregularities. This results in some difference between reality and simulation. In this case, the difference is smaller than 1 mm.
The strong advantage of LPBF of high freedom of geometry can be exploited if the geometry of the capsule is designed in such a way that, after HIP, the final geometry of the component has already been achieved without post-processing. To achieve this goal, the geometry of the capsule can be iteratively optimized. This optimized geometry can then easily be loaded into the LPBF unit in a digital exchange format.

© European Powder Metallurgy Association (EPMA)

The flowchart of this iterative geometry optimization is shown in Figure 17: First the model is built according to target geometry. This model is then simulated using the aforementioned HIP simulation routine. In the following step, the outcome of this first simulation is compared to the target geometry. The absolute value of each deviation is added with the opposite sign to the capsule's geometry. This operation expands the capsule by a certain amount. After this expansion, the geometry is once again simulated.
The final iteration is reached when the difference of the respective coordinates of each node between two steps is smaller than a previously specified error. The capsule geometry prior to simulation of this very last iteration is the target geometry to be LPBF built.

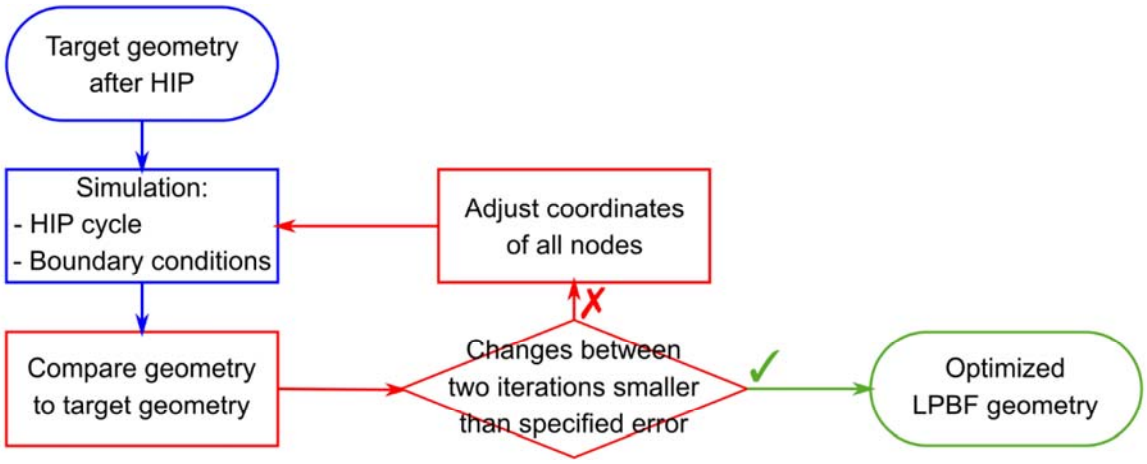


Figure 17: Flowchart of numerical geometry optimization of LPBF capsule.

The iterative geometry optimization in order to reach a cylindrical capsule is shown in Figure 18. Starting with a cylindrical shape (top left), the first HIP simulation step yields a concave-shaped capsule (bottom left). The coordinates of all nodes are expanded (top center). After the second simulation step, the shape is more in line with the target geometry. After two more iterations (not shown in Figure 18, the geometry after simulation (bottom right) is virtually identical to the target geometry. The geometry of this last step before HIP (top right) is the final geometry for LPBF. For all steps, the filling pipe is part of the model and assumed with full density. The filling pipe is not shown in Figure 18.
As can easily be seen from Figure 18, the values for shrinkage and expansion are highest at the first simulation and iteration step. After this first step, they are much smaller for every following step. Figure 19 left shows shrinkage and expansion for the height of the capsule. The asymptotic course of iterations can be a starting point for economic optimization: If the model is too complex and the simulation or iteration takes too long, not all iterations have to be performed. The lack of accuracy should be acceptable.

© European Powder Metallurgy Association (EPMA)

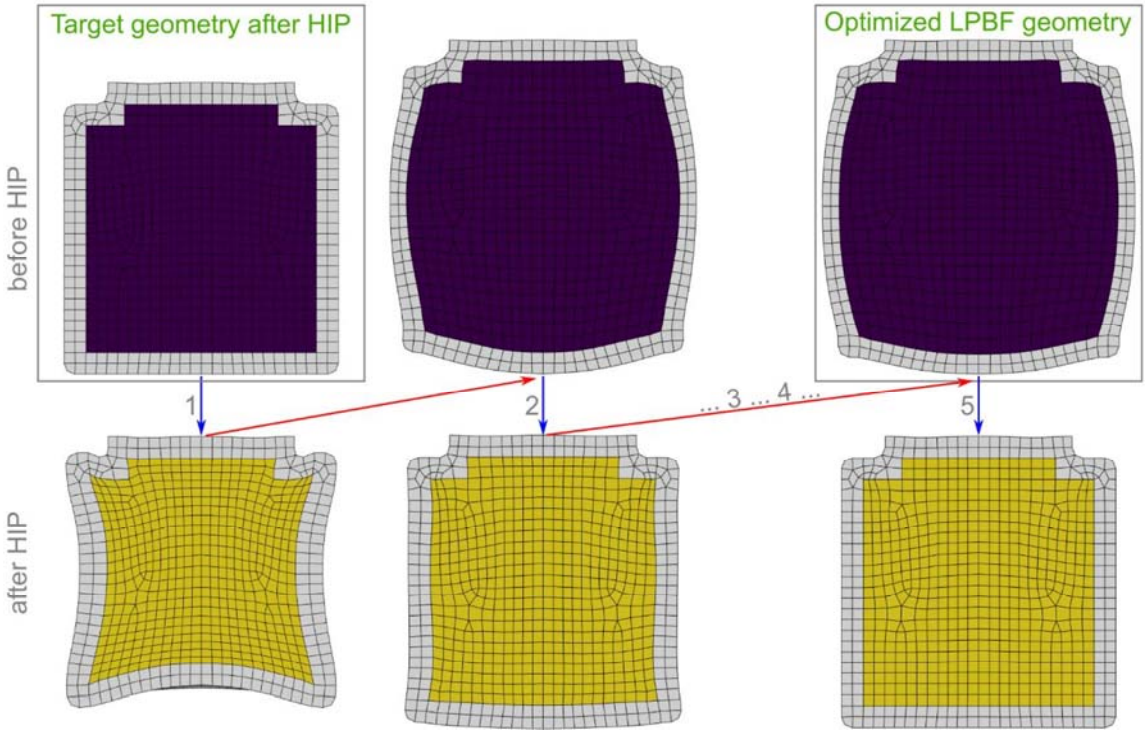


Figure 18: Iterations for net-shape optimization of LPBF capsule (iterations no. 3 and 4 not shown).

In the middle of Figure 19, a cross-cut of the final geometry before HIP is shown. The simulated geometry of the capsule after HIP is shown at the right.

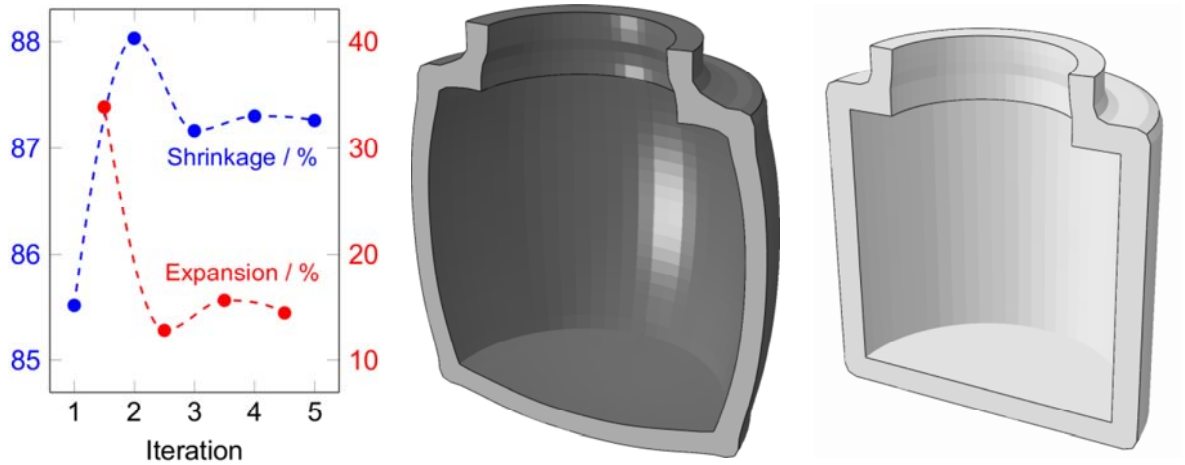


Figure 19: Asymptotic course of iterations for net-shape geometry (left), final capsule geometry before HIP (middle) and after HIP (right). Capsules are shown without filling pipe and powder filling.

This simulation routine for iteratively optimizing the geometry of a HIP capsule can be applied to capsules of any complexity. Figure 20 shows the procedure for an extrusion screw: The initial CAD model has to be equipped with a small socket (a) and transferred to a data format that is suitable for FEM simulation (b). Then the optimization loop according to Figure 17 starts. After a number of iterations (five iterations for the model shown here), the final LPBF geometry has been calculated (c). Applying the HIP simulation according to equation (1) to the optimized capsule, the net-shape geometry after HIP can easily be seen (d).

© European Powder Metallurgy Association (EPMA)

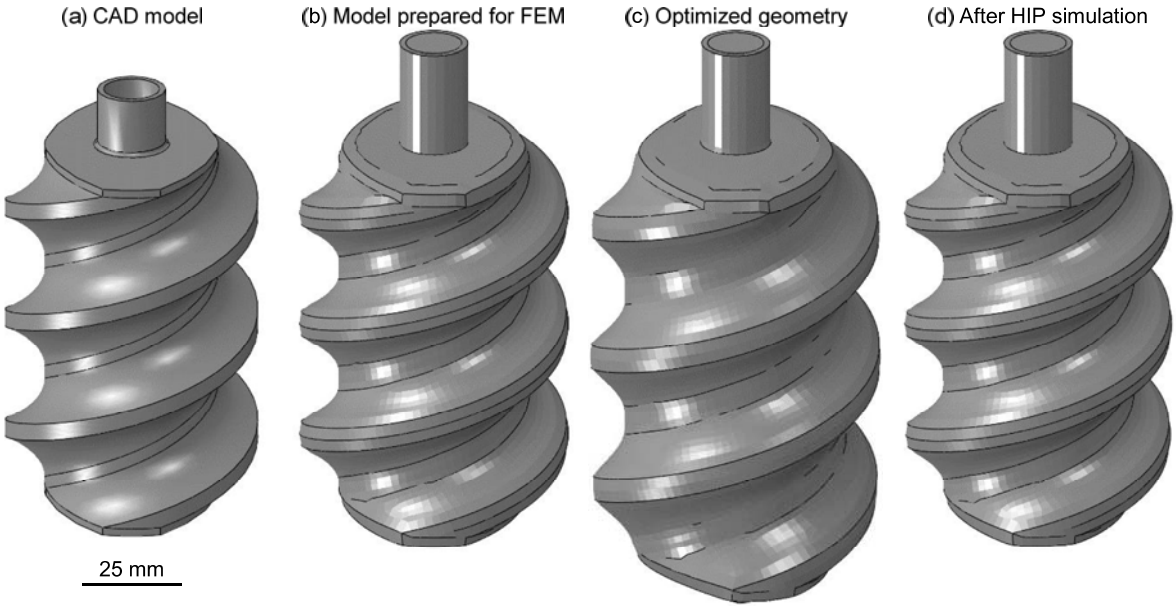


Figure 20: Complex geometry of extrusion screw optimized for LPBF & HIP.

4. Summary and Outlook

The combination of LPBF and HIP offers high potential to produce complex shaped components.
A set of optimal parameters for LPBF of 316L could be determined. Capsules made of 316L were gas tight and could be compacted by HIP. Filling of 316L capsules with 316L powder as well as L6 powder proved successful. Some challenges such as pores after HIP have to be addressed. Mechanical tests must show how the capsules produced this way can prove their reliability despite their process-related properties.
It has been shown that high-carbon steel A11 diluted with low carbon ferritic steel can be successfully processed with LPBF. Simple geometries like cubes could be built. More complex-shaped capsules were destroyed within the first few millimetres of building. The ideal parameter set for producing capsules have yet to be determined.
With the help of numerical FEM simulation the geometry of complex HIP capsules can be optimized with regard to net-shape building. In this study, the optimization of simple cylindrical capsules as well as a complex-shaped geometry were presented. The next step is to LPBF-build the optimised capsules and compare the shape after HIP with the target geometry.

Acknowledgements

The authors would like to thank Bengt Hallstedt and Yuanbin Deng for their respective contributions to this work.
The project with the number 18968 N of FSV e. V. Hagen is funded via AiF within the context of IGF by the Federal Ministry of Economics and Energy thanks to a resolution of the German Bundestag.

Bundesministerium für Wirtschaft und Energie

References

1. Atkinson, H.V., Davies, S.: Fundamental aspects of hot isostatic pressing: An overview. Metall and Mat Trans A (2000). doi: 10.1007/s11661-000-0078-2
2. Yap, C.Y., Chua, C.K., Dong, Z.L., Liu, Z.H., Zhang, D.Q., Loh, L.E., Sing, S.L.: Review of selective laser melting. Materials and applications. Applied Physics Reviews (2015). doi: 10.1063/1.4935926
3. Sundaram, M.V.: Processing Methods for Reaching Full Density Powder Metallurgical Materials, 111/2017. Department of Materials and Manufacturing Technology Chalmers University of Technology, Gothenburg (2017)
4. Smarsly, W., Lee, Y.T., Welsch, G.: Microporosity in hot isostatically pressed Ti-6Al-4V powder compacts. MTA (1985). doi: 10.1007/BF02670370
5. Bocanegra-Bernal, M.H.: Hot Isostatic Pressing (HIP) technology and its applications to metals and ceramics. Journal of Materials Science (2004). doi: 10.1023/B:JMSC.0000044878.11441.90

© European Powder Metallurgy Association (EPMA)

6. Berglund, T., Östlund, M., Larsson, L.: Impact Toughness of PM HIP'ed vs. Conventional 316L. In: European Powder Metallurgy Association (ed.) Euro PM2015 Proceedings. Euro PM2015, Reims, 4.–7.10.2015 (2015)
7. Broeckmann, C., Güthoff, T., Wünsch, H., Bengtsson, B.O., Volker, K.-U.: Zähigkeit von Duplexstahl, hergestellt durch Pulver-HIP (2013)
8. Wroe, J.: Introduction to Hot Isostatic Pressing Technology. A guide for Designers and Engineers. EPMA, Shrewsbury, UK. https://www.epma.com/epma-free-publications/product/introduction-to-hot-isostatic-pressing-brochure (2014)
9. Wroe, J.: Introduction to Additive Manufacturing Technology. A guide for Designers and Engineers. EPMA, Shrewsbury, UK (2015)
10. DIN: Determination of solid state density – Part 2: Gaspycnometry. Beuth Verlag GmbH **17.060**(DIN 66137-2) (2018)
11. Atkinson, H.V., Rickinson, B.A.: Hot isostatic processing. The Adam Hilger series on new manufacturing processes and materials. Hilger, Bristol (1991)
12. Jeon, Y.C., Kim, K.T.: Near-net-shape forming of 316L stainless steel powder under hot isostatic pressing. International Journal of Mechanical Sciences (1999). doi: 10.1016/S0020-7403(98)00053-8
13. Van Nguyen, C.: Numerical Simulation of Hot Isostatic Pressing with Particular Consideration of Powder Density Distribution and Temperature Gradient, 1st edn. Werkstoffanwendungen im Maschinenbau, vol. 11. Shaker, Herzogenrath (2016)
14. Cooper, A.J., Cooper, N.I., Dhers, J., Sherry, A.H.: Effect of Oxygen Content Upon the Microstructural and Mechanical Properties of Type 316L Austenitic Stainless Steel Manufactured by Hot Isostatic Pressing. Metall and Mat Trans A (2016). doi: 10.1007/s11661-016-3612-6
15. Schindelin, J., Arganda-Carreras, I., Frise, E., Kaynig, V., Longair, M., Pietzsch, T., Preibisch, S., Rueden, C., Saalfeld, S., Schmid, B., Tinevez, J.-Y., White, D.J., Hartenstein, V., Eliceiri, K., Tomancak, P., Cardona, A.: Fiji: an open-source platform for biological-image analysis. Nature methods (2012). doi: 10.1038/nmeth.2019
16. DIN: Steel – Micrographic determination of the apparent grain size. Beuth Verlag GmbH, Berlin **77.040.99**(DIN EN ISO 643) (2017)
17. Kuhn, H.A., Downey, C.L.: Deformation Characteristics and Plasticity Theory of Sintered Powder Materials. International Journal of Powder Metallurgy **7**(1), 15–25 (1971)
18. Abouaf, M., Chenot, J.L., Raisson, G., Bauduin, P.: Finite element simulation of hot isostatic pressing of metal powders. Int. J. Numer. Meth. Engng. (1988). doi: 10.1002/nme.1620250116
19. Geenen, K., Röttger, A., Theisen, W.: Corrosion behavior of 316L austenitic steel processed by selective laser melting, hot-isostatic pressing, and casting. Materials and Corrosion (2017). doi: 10.1002/maco.201609210
20. Lou, X., Andresen, P.L., Rebak, R.B.: Oxide inclusions in laser additive manufactured stainless steel and their effects on impact toughness and stress corrosion cracking behavior. Journal of Nuclear Materials (2018). doi: 10.1016/j.jnucmat.2017.11.036
21. Lemke, J.N., Casati, R., Lecis, N., Andrianopoli, C., Varone, A., Montanari, R., Vedani, M.: Design of Wear-Resistant Austenitic Steels for Selective Laser Melting. Metall and Mat Trans A (2018). doi: 10.1007/s11661-017-4461-7
22. Herzog, D., Seyda, V., Wycisk, E., Emmelmann, C.: Additive manufacturing of metals. Acta Materialia (2016). doi: 10.1016/j.actamat.2016.07.019
23. Deutsche Edelstahlwerke GmbH: FeCrV10 ZTU-Schaubild für kontinuierliche Abkühlung, Witten

© European Powder Metallurgy Association (EPMA)